Bull Volcanol (2007) 69:769–784
DOI 10.1007/s00445-006-0107-0

RESEARCH ARTICLE

Strombolian explosive styles and source conditions: insights from thermal (FLIR) video

Matthew R. Patrick · Andrew J. L. Harris · Maurizio Ripepe · Jonathan Dehn · David A. Rothery · Sonia Calvari

Received: 2 September 2005 / Accepted: 13 September 2006 / Published online: 9 January 2007

Abstract Forward Looking Infrared Radiometer (FLIR) cameras offer a unique view of explosive volcanism by providing an image of calibrated temperatures. In this study, 344 eruptive events at Stromboli volcano, Italy, were imaged in 2001–2004 with a FLIR camera operating at up to 30 Hz. The FLIR was effective at revealing both ash plumes and coarse ballistic scoria, and a wide range of eruption styles was recorded. Eruptions at Stromboli can generally be classified into two groups: Type 1 eruptions, which are dominated by coarse ballistic particles, and Type 2 eruptions, which consist of an optically-thick, ash-rich plume, with (Type 2a) or without (Type 2b) large numbers of ballistic particles. Furthermore, Type 2a plumes exhibited gas thrust velocities (>15 m s^{-1}) while Type 2b plumes were limited to buoyant velocities (<15 m s^{-1}) above the crater rim. A given vent would normally maintain a particular gross eruption style (Type 1 vs. 2) for days to weeks, indicating stability of the uppermost conduit on these timescales. Velocities at the crater rim had a range of 3–101 m s^{-1}, with an overall mean value of 24 m s^{-1}. Mean crater rim velocities by eruption style were: Type 1= 34 m s^{-1}, Type 2a=31 m s^{-1}, Type 2b=7 m s^{-1}. Eruption durations had a range of 6–41 s, with a mean of 15 s, similar among eruption styles. The ash in Type 2 eruptions originates from either backfilled material (crater wall slumping or ejecta rollback) or rheological changes in the uppermost magma column. Type 2a and 2b behaviors are shown to be a function of the overpressure of the bursting slug. In general, our imaging data support a broadening of the current paradigm for strombolian behavior, incorporating an uppermost conduit that can be more variable than is commonly considered.

Keywords FLIR · Stromboli volcano · Monitoring · Thermal imaging · Eruption dynamics

Editorial responsibility: R Cioni

M. R. Patrick · A. J. L. Harris
Hawaii Institute of Geophysics and Planetology,
School of Ocean and Earth Science and Technology,
University of Hawaii Manoa,
1680 East–West Road,
Honolulu, HI 96822, USA

M. R. Patrick · D. A. Rothery
Department of Earth Sciences, The Open University,
Walton Hall,
Milton Keynes MK7 6AA, UK

M. Ripepe
Dipartimento di Scienze della Terra, Universita di Firenze,
Via G. La Pira,4,
Firenze I-50121, Italy

J. Dehn
Alaska Volcano Observatory, Geophysical Institute,
University of Alaska Fairbanks,
903 Koyukuk Drive,
Fairbanks, AK 99775, USA

S. Calvari
Istituto Nazionale di Geofisica e Vulcanologia,
Piazza Roma 2,
Catania 95123, Italy

M. R. Patrick (✉)
Department of Geological and Mining Engineering and Sciences,
Michigan Technological University,
1400 Townsend Drive,
Houghton, MI 49931, USA
e-mail: mpatrick@mtu.edu

Introduction

Stromboli volcano, in the Aeolian Islands of Italy, offers an excellent location to study mildly explosive basaltic volcanism due to its eruptive frequency and ease of access. It serves as the archetype for 'strombolian' activity, an eruptive behavior common to many other volcanoes (e.g. Shishaldin, Fuego, Villarrica, Etna, Karymsky). Through seismicity (e.g. Ntepe and Dorel 1990), infrasound (e.g. Ripepe and Marchetti 2002), geochemistry (e.g. Francalanci et al. 2004), laboratory models (e.g. Jaupart and Vergniolle 1988; Ripepe et al. 2001), physical volcanology (e.g. Lautze and Houghton 2005) and assorted other tools, our understanding of Stromboli's eruption dynamics has improved substantially over the last 30 years. Ground-based imaging (Chouet et al. 1974; Blackburn et al. 1976; Ripepe et al. 1993) has also proven to be an important tool, providing information on the surface manifestation, and end products, of the eruptive process.

Previous imaging studies at Stromboli (Chouet et al. 1974; Blackburn et al. 1976; Ripepe et al. 1993) suffer from two shortcomings. First, the inherent limitations of visible and near-infrared photography preclude simultaneous observation of major ejecta constituents. If viewing at night, the incandescent ballistic particles will be visible but the generally low-temperature ash plume, if present, will be largely invisible. During daylight, any ash plume will be conspicuous but ballistic particles, due to their small size, can be distinguished only at a high magnification which then eliminates a synoptic view of the eruption. Second, each study considered a small dataset (a combined total of <30 eruptions) collected over a short time period and, therefore, they may not characterize the entire suite of normal strombolian activity. In spite of the small data sets, the results from these studies have served as supportive, and at times fundamental, data for a number of models of Stromboli's eruption and conduit dynamics (e.g. McGetchin and Chouet 1979; Wilson 1980; Giberti et al. 1992; Allard et al. 1994; Vergniolle and Brandeis 1994; Harris and Stevenson 1997; Parfitt 2004). This underlines the importance of exploring the degree to which these imaging studies convey the full range of normal strombolian activity.

In this study we use a Forward Looking Infrared Radiometer (FLIR) handheld camera to characterize strombolian eruptions. The FLIR produces temperature-calibrated thermal images capable of capturing the ballistic particles as well as any ash plume within a field of view (~140 m high at 450 m distance) that offers a synoptic view of the eruption. During May 2001, May 2002, September 2003, and June–July 2004, 344 strombolian eruptions were imaged, and the data were analyzed in order to characterize and understand the variability of eruptive behavior at Stromboli.

Conceptual model of strombolian eruptions

Eruptions at Stromboli, as well as strombolian eruptions at other volcanoes, are commonly thought to originate from the bursting of a gas slug at the magma free surface (Macdonald 1972; Chouet et al. 1974; Blackburn et al. 1976; Jaupart and Vergniolle 1988; Ripepe et al. 1993; Vergniolle and Brandeis 1994, 1996). As early as the eruption of Parícutin in 1943–1952, Foshag and Gonzalez-Reyna (1956) remarked on 'Huge bubbles... presumably filled with gases. When they burst, huge glowing masses of viscous lava were flung over the cone.' The mechanism of gas slug formation has been a point of debate centered around two primary models (see Parfitt 2004 for review). In the first—a collapsing foam model (Jaupart and Vergniolle 1988; Vergniolle and Brandeis 1994, 1996)—the slug originates from an accumulation of small bubbles, or foam, at the roof of a magma reservoir. At a critical point, the foam collapses and a large gas slug coalesces and subsequently travels up the conduit. In the second—a rise-speed dependent model (Wilson 1980; Parfitt and Wilson 1995)—bubbles of many original sizes buoyantly rise within a column of upward rising magma. If the magma rise velocity and viscosity are low, bubbles can travel a sufficient distance to interact with one another, allowing larger bubbles (which travel faster) to overtake and coalesce with smaller ones traveling slower. This has a compounding effect and a large gas slug is eventually formed.

Regardless of the model, seismic evidence suggests that a volumetric expansion of the gas slug at Stromboli occurs at an approximate depth of 250 m (Kirchdorfen 1999; Chouet et al. 1999, 2003; Marchetti and Ripepe 2005), suggesting slug coalescence occurs at or below that depth. Viscous forces inhibit perfect equilibration of the pressure inside the slug during its ensuing ascent and it arrives at the magma free-surface with a minor amount of overpressure, typically ~0.5–4 b (Ripepe and Marchetti 2002). The overpressure bursts the gas slug, with the force of the gas explosion ejecting coarse fragments of the molten lava that had surrounded the slug (Walker 1973; Blackburn et al. 1976). Many of the particles are incandescent, resulting in the brilliant parabolic trajectories that are characteristic of strombolian eruptions. These coarse particles are lapilli to bomb size (~2–30 cm, Chouet et al. 1974; Ripepe et al. 1993), typically ejected to heights of several hundred meters, and generally fall within a few hundred meters of the vent.

Some strombolian explosions erupt finer particles which couple with the gas phase, creating an ash plume. The high initial velocities of the gas thrust phase decline to the roughly constant velocities of the buoyant convective phase; in several strombolian eruptions at Heimaey this transition height was 80–150 m (Sparks and Wilson 1976).

At Stromboli, Blackburn et al. (1976) measured initial plume velocities of 28–65 m s^{-1} and convective velocities of 4–8 m s^{-1}.

Strombolian eruptions thus eject a mixture of both volcanic gas and particles. The particles can comprise a range of different size fragments from ash to bombs. Fine particles remain mechanically coupled to the gas phase to form an ash plume. Coarser particles follow a trajectory that is largely independent of the dynamics of the gas phase, although the path can be modified initially by the ascending gas (Self et al. 1980). We loosely refer to coarse particles in this study as 'ballistic' because most appeared decoupled from the gas phase, following roughly parabolic trajectories.

Data collection

FLIR ThermaCAM™ cameras

We used three different FLIR camera models, all produced by FLIR Systems, Inc., to image the eruptions. The first was a ThermaCAM™ PM 595 model, which uses an uncooled microbolometer detector array with a field of view of 24°×18°, an instantaneous field of view of 1.3 mrad, and a thermal response from 7.5 to 13 μm. Acquisition occurs at 60 Hz (60 frames per s), but image storage on this model can be achieved only at a 2 s interval (0.5 Hz). The images are 320×240 pixels (76,800 data points) at 14 bit quantization, producing an image file size of ~150 kB. The second camera was a ThermaCAM™ PM 695, which is essentially identical to the PM 595. The third camera, a ThermaCAM™ S40, is also similar to the PM 595 in most respects with the exception that it can save imagery at 30 Hz via Firewire to a notebook computer (Fig. 1). On several occasions we used two S40 models simultaneously, one using the standard 24° lens and the other using a 12° lens pointed at the vent area. The FLIR is lightweight (~2 kg with battery) and lacks moving parts (with the exception of the periodic shutter calibration mechanism), making it well-suited for the field (Dehn et al. 2001).

FLIR measurement setup

The FLIR data used in this study were collected over four field seasons: 17 May–02 June 2001, 09 May–25 May 2002, 16 Sept 2003, and 05 June–25 July 2004 (Table 1). A total of 344 eruptions was recorded, with the majority (240) being obtained during the 2004 campaign. As the 2004 dataset was collected with the S40 model acquiring at 30 Hz, it offered parameterization at an extremely fine timescale. The other large dataset includes 64 eruptions

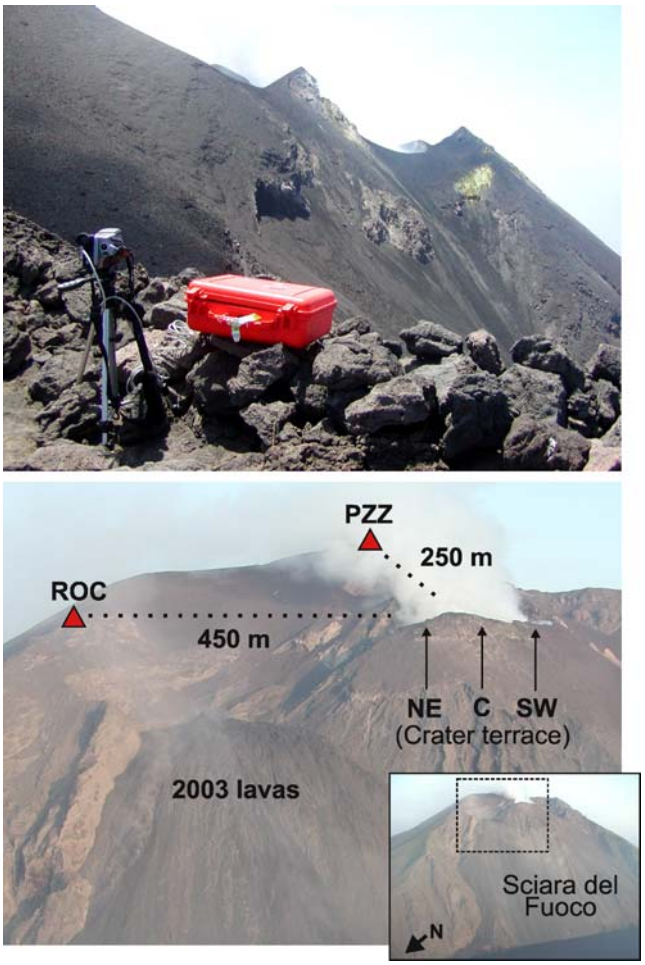

Fig. 1 Recording setup on Stromboli. Top: The FLIR ThermaCAM S40, about the size and weight of a conventional video camera, at the Rocette (ROC) site on Stromboli volcano. The camera is connected via Firewire to a notebook computer, in the orange Pelican case, to collect at 30 Hz. Bottom: The two recording sites relative to the crater terrace. The inset shows a larger scale view of the western side of Stromboli and the Sciara del Fuoco, and extent of the lower photo (*dotted box*). Photo taken in May 2003

acquired during a low-activity period in May 2002. These eruptions, along with those from May 2001 and September 2003, were imaged every 2 s (0.5 Hz). This timescale is much coarser than the 30 Hz data but nonetheless allowed a reasonable characterization of eruption style. The camera was run continuously for typically ~4 h on each observation day to ensure capture of eruption onsets. At 30 Hz, the data rate is ~4.5 MB s^{-1}, or 1 GB every 3–4 min. The camera was tripod mounted for stability.

The camera was placed at either the Pizzo Sopra la Fossa (PZZ) or Roccette (ROC) site (Fig. 1), approximately 250 m and 450 m away from the active craters, respectively. PZZ is about 150 m above the craters, while ROC is approximately level with them. At 250 m and 450 m distance, each pixel in the FLIR image is 33 cm and 59 cm in dimension, respectively. PZZ provides views of all the

Table 1 Explosions imaged by the FLIR camera

	May 17–Jun 02, 2001	May 09–25, 2002	Sep 16, 2003	Jun 05–Jul 25, 2004	Overall
NE eruptions	8	36	2	170	216
C eruptions	0	1	5	9	15
SW eruptions	18	27	7	61	113
Total eruptions	26	64	14	240	344
Imaging frequency (Hz)	0.5	0.5	0.5	30	
Camera	595	595	695	S40	
Location*	PZZ	PZZ	PZZ	ROC + PZZ	

*see Fig. 1 for locations

active craters and was used exclusively in May 2001, May 2002, and September 2003. Being closer to the craters, it allowed features to be imaged at a finer resolution, though its field of view was limited. The vertical height of the image was just ~75 m, so that many eruptions quickly extended beyond the field of view. The ROC site was used most often in June 2004. Although it was farther from the crater terrace and could only image the NE crater without obstruction, its vertical field of view was ~140–180 m (depending on camera orientation). This allowed longer observation of the rising ash plumes. Also, due to a crater floor collapse and loss of the NE wall of the crater terrace in December 2002, the ROC site in 2004 allowed a rare opportunity to see deep into NE crater, thereby allowing us to capture the ejecta much closer to the vent than in other periods. Eruptions in 2001–2002 were captured after dark, while those in 2003 and 2004 were imaged during the daytime.

Each explosion originated from one of three main craters (SW, Central and NE) in a 300 m long crater terrace (Figs. 1 and 2). At the onset of the 2002–2003 effusive phase in December 2002 much of the terrace collapsed, destroying the septa and inner flanks that had distinguished the Central and NE craters (Calvari et al. 2005). Although the crater edifices were no longer in place the approximate vent locations remained intact, and by the end of the effusive eruption in July 2003 the craters were reforming in their pre-2003 locations (Calvari et al. 2005).

Of the 344 eruptions imaged, 113 were from SW crater. The Central crater only rarely produced what would be considered typical strombolian explosions. Just 15 eruptions were observed at Central crater, and these were extremely small in size. The NE crater was separated into several sub-craters, which we refer to as NE-1, NE-2, and NE-3 (Fig. 2). During May 2002 and June–July 2004, NE crater was the most active and the camera was pointed at this crater more often than the others, with a total of 216 eruptions imaged. Because the FLIR field of view could accommodate only 1–2 craters at a time during 2001, 2002 and 2003, the number of imaged eruptions for each crater is partly a measure of where the camera was pointed, and not the relative eruption frequency.

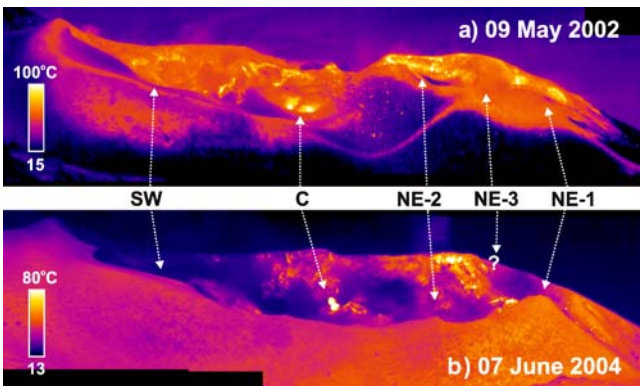

Fig. 2 The crater terrace as viewed from the Pizzo sopra la Fossa (~250 m distance, see Fig. 1). Crater/vent locations are shown for May 2002 (**a**) and June 2004 (**b**). The elevated temperatures on the outer flanks of the crater terrace in (**b**) result from solar heating. Each image is ~300 m wide

FLIR sensitivity to ballistic particle size

Chouet et al. (1974) and Ripepe et al. (1993) determined that most strombolian ballistic particles are less than 30 cm in diameter, suggesting that the majority of the ballistic particles we image with the FLIR are subpixel (<60 cm) in size. The ballistic particle size sensitivity was calculated using the Planck function, while incorporating the spectral response function provided by FLIR Systems, Inc. Considering the variability in background temperatures, we judged that a pixel-integrated temperature contrast of 5°C is a conservative threshold for reliable visual identification of ballistic pixels. At a distance of 450 m and background temperatures of 0–20°C, this equates to particle sizes of 2.1(±0.1) and 3.5(±0.2) cm for particle temperatures of 1,000 and 500°C, respectively. At 250 m, this equates to 1.2(±0.1) and 1.9(±0.1) cm for temperatures of 1,000 and 500°C, respectively. This calculation only applies to solitary coarse particles—in ash

plumes the particle size is much smaller, but the particle concentration typically produces an opaque plume that spatially fills the pixel.

Methods of analysis

Qualitative observations

Naked-eye and audible observations comprised the first step in characterizing eruption styles and were especially valuable in 2004, when acquisitions were performed in daytime. Data were collected during daylight hours during September 2003 as well, but they comprised a relatively small dataset (14 eruptions). During other periods (2001–2002), the eruptions were captured after dark, when ballistics were visible clearly due to their incandescence but ash plumes could not be seen. These observations augmented insights from the FLIR video sequences, viewed with ThermaCAM™ Researcher. The presence or absence of an optically-thick ash plume, and the abundance of ballistic ejecta, were used as discriminating characteristics for eruption style. The FLIR proved more effective than naked-eye observations at conveying the full dispersal range of ballistic ejecta during daytime, and improved the viewing of ash plumes during nighttime.

Plume front tracking

Ash plume heights were measured at their leading front using the FLIR imagery. In ballistic-rich (ash-poor) eruptions, plumes became diffuse and invisible too early to track for an extended distance. The method was applied to 80 ash plumes in June–July 2004 (NE-1 crater), in which the vertical field of view was either ~130 m or ~180 m depending on camera orientation. Height values were measured every 3–5 frames (or every 0.08–0.16 s at 30 Hz acquisition) in the gas thrust region and every 10–30 frames (0.33–1 s) in the slower convective region. These apparent height values were then corrected for minor vertical distortions (<3%) due to camera viewing angle. For calculating velocity and acceleration, the height values through time were fit with a fifth-order polynomial. More details on the plume measurements can be found in Patrick (2007).

Plume velocity at crater rim

The velocity of the gas/ash plume onset for 134 eruptions from NE-1 crater during June–July 2004 was measured from the FLIR imagery over a small distance (mean: 9.5 m) and short time interval (mean: 0.7 s) just above the crater rim. Plumes were used for this measurement, because each can be treated as a single, easily-tracked object with a spatial scale larger than the FLIR pixels. Ballistic velocities, on the other hand, depend on particle size (Chouet et al. 1974; Steinberg and Babenko 1978) which could not be measured accurately from the FLIR images due to the coarse pixel size. Although ballistic-rich eruptions lacked an ash-rich plume, their gas plume was discernable very close to the crater rim where gas concentrations presumably were high. In some cases the ballistic particles and plume appeared intermingled and were difficult to discriminate due to the coarse pixel size of the FLIR. These measurements should therefore be considered rough estimates of plume velocity. Also, the actual initial gas velocity at the source will be greater than the plume velocity at the crater rim, as a function of the potentially variable depth of the magma free surface beneath the rim.

Ballistic height

The maximum observed height of ballistics was measured from the imagery for 138 eruptions from NE-1 crater during June–July 2004. A limitation of the FLIR images is that the field of view extended to only 115–180 m above the crater rim, depending on camera orientation. Forty-three (31%) of the eruptions had maximum ballistic heights beyond the top of the field of view. To be consistent, we assigned a value of >115 m to heights that exceeded the field of view, be it 115 or 180 m.

At 450 m distance, the FLIR ballistic particle size sensitivity extends down to 2.1 and 3.5 cm for ballistic temperatures of 1,000 and 500°C, respectively ("FLIR sensitivity to ballistic particle size"). Using a drag coefficient of 1 (Sparks et al. 1997) and mean ballistic density of 1,100 kg m^{-3} (Lautze, 2005, personal communication), initial velocities <100 m s^{-1} will require that ballistics which reach >115 m in height be >7 cm in diameter. Thus, we can be confident that no unaccounted particles were exceeding the field of view.

Eruption duration

Eruption duration was calculated for 135 eruptions from NE-1 crater in June–July 2004 using the FLIR video. The onset of eruption was impulsive and easily identified in all cases. The end of ballistic-rich eruptions was indicated relatively clearly by the final ejection of ballistic particles. The end of ash-rich eruptions could be ambiguous, however, as the trailing portions of the ash plume often stagnated inside the crater and made it difficult to tell if vigorous ejection had finished. The most effective method to identify the end of ash-rich eruptions entailed plotting the maximum temperature in a small (~20 m diameter) window, placed at the crater rim, throughout the course of the eruption. This seemed to produce a good proxy for the

mass flux of hot material passing the crater rim, with an abrupt drop in maximum temperature typically marking the end of an eruption.

Results

The 2001–2003 data, in which all three craters were imaged from an unobstructed viewpoint (PZZ), were used mainly for qualitative assessments of eruption style due to the relatively few eruptions (104) and low frame rate (0.5 Hz). The 2004 field season, in which the camera was pointed at NE crater (but had an obstructed view of Central and SW craters), resulted in the highest quality dataset of our study (in terms of number of eruptions, 240, and camera frame rate, 30 Hz), and we relied on the NE crater eruptions for quantitative results. This section of the paper therefore combines qualitative insights on eruptive behavior from 2001–2004 ("Styles of eruption at Stromboli" and "Style timescales and crater behavior") with a quantitative analysis of eruption dynamics for the best-viewed and most active subcrater (NE-1) during the 2004 field season ("Plume height, velocity and acceleration trends", "Plume velocity at crater rim", "Maximum ballistic height", "Eruption duration").

Styles of eruption at Stromboli

Eruptions varied widely in style and appearance but can be broadly categorized into two main groups: Type 1 (ballistic-dominated) and Type 2 (ash-dominated) eruptions. This scheme is very similar to the two-part classifications of Ripepe et al. (1993), Chouet et al. (1999, 2003), Ripepe and Marchetti (2002) and Marchetti and Ripepe (2005). Their Type 1 and 2 equivalents were based on general appearance as well as the seismic and infrasonic waveforms, and all of these authors attributed Type 1 eruptions to NE crater and Type 2 eruptions to SW crater. Our use of this scheme encompasses only the eruption appearance, and we do not explore seismicity or infrasound in detail. Overall, our results show that both eruption styles were common at both craters (Table 2).

Table 2 Eruption style at the active craters

Month of eruption	Locations of eruption				
May 2001	SW*	C	NE-1	NE-2	NE-3
Type 1	15	0	3	2	2
Type 2a	0	0	0	0	0
Type 2b	12	0	0	0	1
May 2002	SW	C	NE-1	NE-2	NE-3
Type 1	4	1	14	5	1
Type 2a	18	0	0	1	0
Type 2b	5	0	10	3	2
Sept 2003	SW	C	NE-1	NE-2	NE-3
Type 1	7	0	2	0	0
Type 2a	0	4	0	0	0
Type 2b	0	1	0	0	0
Jun–Jul 2004	SW	C	NE-1	NE-2	NE-3
Type 1	0	4	53	12	0
Type 2a	6	2	49	1	0
Type 2b	55	3	44	11	0

*Dual vent eruptions were counted separately for the purposes of eruption style

Type 1 eruptions were ballistic-dominated, with plumes that were only faintly visible just above the crater rim (Fig. 3). A significant plume must be present due to the gas slug, but the paucity of ash-sized particles makes it difficult to discern with either the naked eye or the FLIR. Type 2 eruptions were also common in our study period. This style involves a conspicuous ash plume, the high optical thickness of which often visually obscured many of the ballistic particles (Fig. 3). We found that Type 2 eruptions can be subdivided into two groups: Type 2a, which exhibited a visible gas thrust phase and usually expelled significant ballistics, and Type 2b, which exhibited only convective velocities visible above the crater rim and ejected a minor amount of ballistic particles. Type 2a crater rim velocities overlapped with those of Type 1 activity. Type 2b eruptions, however, were consistently smaller in size and had lower crater rim velocities. Type 1 and 2a eruptions were often very loud, while Type 2b eruptions were commonly inaudible.

There was significant variety within both Type 1 and 2 eruption styles (Fig. 4). Some eruptions were poorly-collimated explosions that seemed to originate close to the crater rim (Fig. 4a), while others were well-collimated and hence may have come from deeper levels (Self et al. 1974) (Fig. 4e). Some were simply small in size (Fig. 4f), while others were moderately (Fig. 4d) to impressively large (Fig. 4b). Some Type 2 eruptions contained a small (Fig. 4f) to moderate (Fig. 4b) amount of ash in their plumes, while others were visibly ash-laden and displayed significant sedimentation (Fig. 4c).

Style timescales and crater behavior

We observed consistency in eruption style through time for a given vent. With only several clear exceptions (described below), the gross eruption style (Type 1 vs. 2) was maintained throughout each 2–5 h observation period at a particular vent. Although we lack continuous data over longer periods, we observed consistency in gross style among observation days that suggests a persistence over days to weeks. Our best coverage comes from the 2004 dataset, due to a high number of collected eruptions and coverage of both NE and SW craters (again, note that SW crater was partially obscured in this setup, allowing style

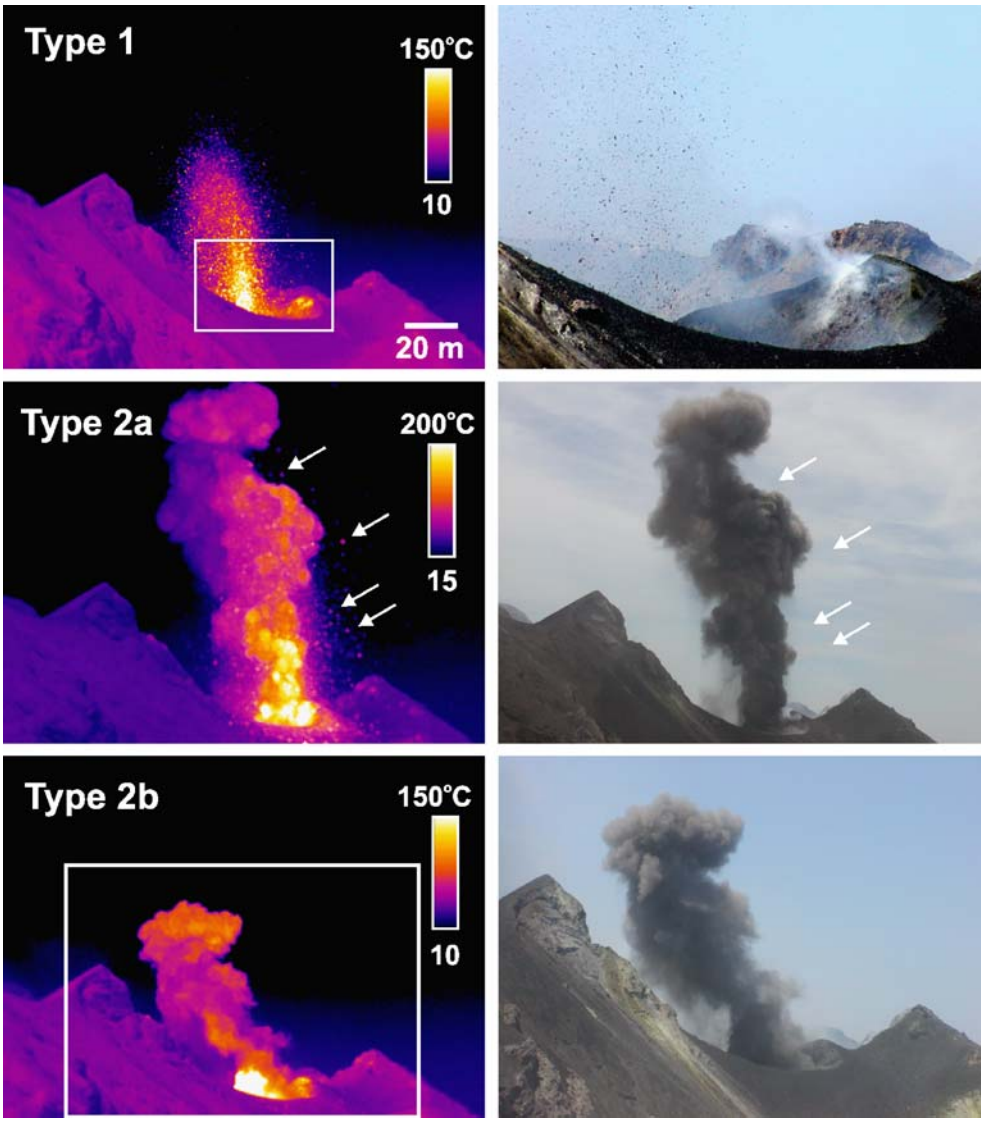

Fig. 3 The main types of eruptions at Stromboli. Type 1 eruptions are ballistic-dominated, with little to no visible plume due to the absence of ash-sized particles. Type 2 eruptions involve emission of an ash plume, with Type 2a containing significant ballistic particles and Type 2b having few ballistics. Notice the skirt of particles at the base of the Type 2a plume, and several large airborne particles marked by *arrows*. *White boxes* show corresponding photo area, and the spatial scale is identical in all three FLIR images. The Type 2a FLIR image has been enhanced slightly to make the ballistic particles more obvious for print

discrimination but not quantitative analyses). For SW crater, Type 2 activity (predominantly Type 2b) exclusively was observed on all 13 acquisition days in 2004; this suggests Type 2 style was maintained throughout those 2 months. At NE-1 crater, activity was more variable but nonetheless exhibited consistency among observation days. The first observation day, June 05, consisted of Type 1 eruptions. The next observation day, June 07, consisted of Type 2 eruptions, which were subsequently observed on June 09, 11, 13, 19 and 27. Type 1 activity was noted by others (Palma, 2005, personal communication) on the summit on July 05, and the next observation day, July 07, had Type 1 activity which was also present on July 11, 14 and 18. Eruptions on July 20 were Type 2, as well as those on July 25. These observations suggest that eruption styles were maintained at NE-1 crater for days to possibly several weeks at a time.

In several cases, both Type 1 and 2 styles were noted for the same vent during a single observation period, owing to both observational limitations and real changes. First, our Type 1–2 classification is based upon visual appearances, and thus some eruptions could challenge a clear visual distinction. This was the case on July 25, 2004, when most eruptions were deemed Type 2 (and visible film confirms an ash plume was present) but had ash plumes of a relatively low optical thickness. Two of the least ash-charged eruptions on this day better resembled Type 1 eruptions and were assigned as such. Several eruptions in May 2002 were problematic for this reason as well, aggravated in part by their small volume of ejecta. On the other hand, unequivocal changes in eruption style on the same day were noted on only two occasions. The best example was on July 18, 2004 at NE-1 crater. A 3.5-hour-long series of 10 low-intensity Type 1 eruptions was

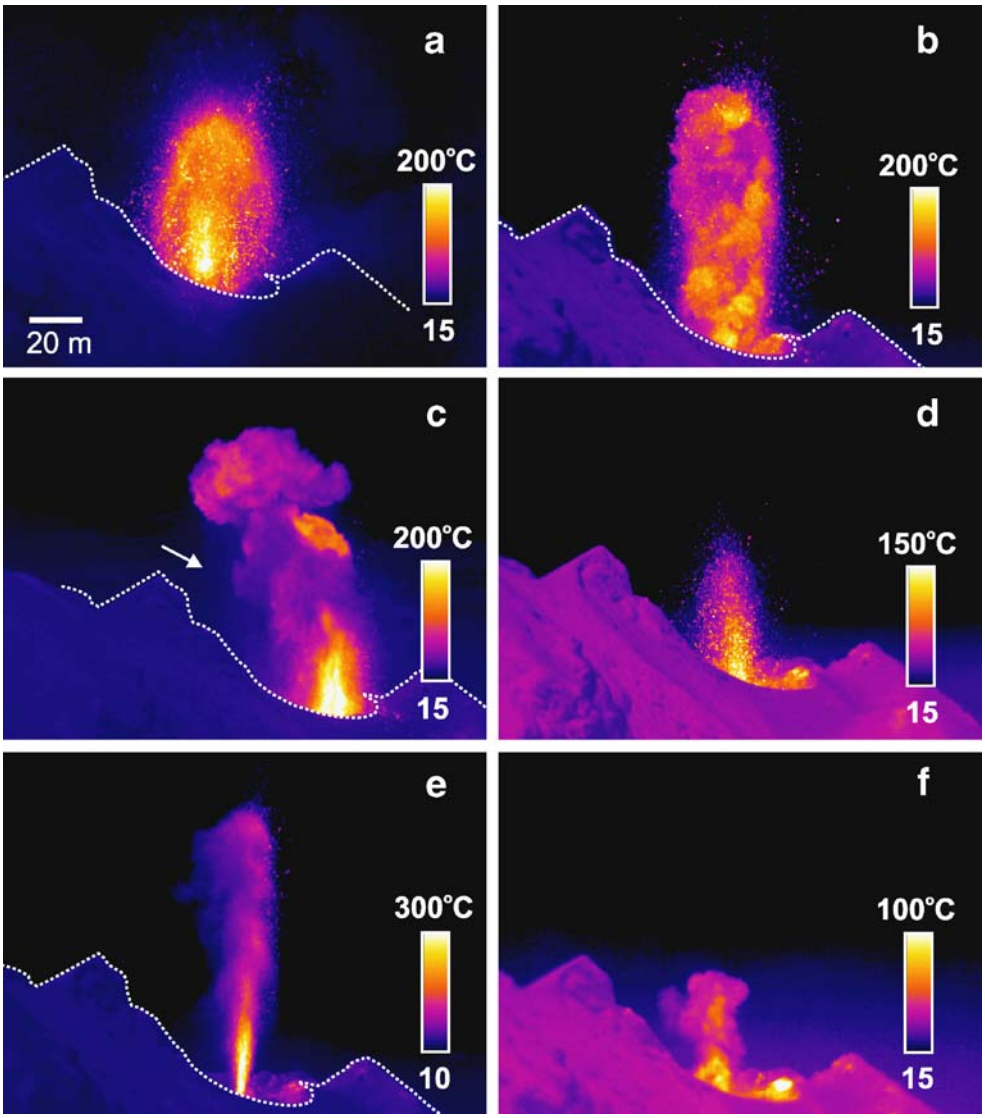

Fig. 4 The varying styles of eruptions at Stromboli. **a** Type 1 eruption, with poor collimation, 5 June 2004, **b** Type 2a eruption with high-velocity ash plume, 7 June 2004, **c** Type 2b eruption with low-velocity, particle-laden plume and high degree of visible sedimentation, 13 June 2004. Arrow points to sedimentation cloud. **d** Mild Type 1 eruption with moderate collimation, 7 July 2004. **e** Intense Type 1 eruption, with excellent collimation, 14 July 2004. **f** Small Type 2b eruption, 18 July 2004. Spatial scale is identical in all images. All eruptions originate from NE-1 crater

followed, after an interval of 22 min, by three robust Type 2 eruptions within the next 30 min. Forty minutes after the last Type 2 eruption, activity reverted to the original Type 1 style.

Type 2a and 2b eruptions originating from the same vent on the same day were common and often alternated on a timescale of minutes. For instance, on June 13, 2004, ten Type 2b and four Type 2a eruptions took place from NE-1 crater within ~3 h. The Type 2a minority was reasonably well distributed among the Type 2b eruptions in this case, with each Type 2a preceded by a Type 2b eruption.

Plume height, velocity and acceleration trends

Type 2a eruptions are defined as those having a visible gas thrust phase, and Type 2b eruptions as those with only buoyant velocities visible above the crater rim. Buoyant phases, evident from their lack of deceleration, had a peak velocity of 11 m s^{-1} among the eruptions we analyzed, and so we choose the rough lower limit for gas thrust velocities as 15 m s^{-1}.

Figure 5 shows plume height trends for 80 NE-1 crater ash plumes in 2004. The height versus time plots show the original data points, while the velocity and acceleration plots were produced from polynomial-smoothed data. Note that the fifth-order polynomial used for smoothing assumes reasonably smooth velocity and acceleration trends for simplicity; higher-order polynomials would be required to characterize more rapid changes which may be present.

The fundamental difference between Type 2a (gas thrust) and Type 2b (buoyant) styles is shown in Fig. 5. Velocities for Type 2a eruptions could reach up to 50 m s^{-1} at the crater rim and decelerated (at a rate of up to 30 m s^{-2}) to buoyant velocities (<15 m s^{-1}) within 100 m above the rim. Notice that velocities remained roughly constant once buoyant velocities were attained. Type 2b eruptions lacked

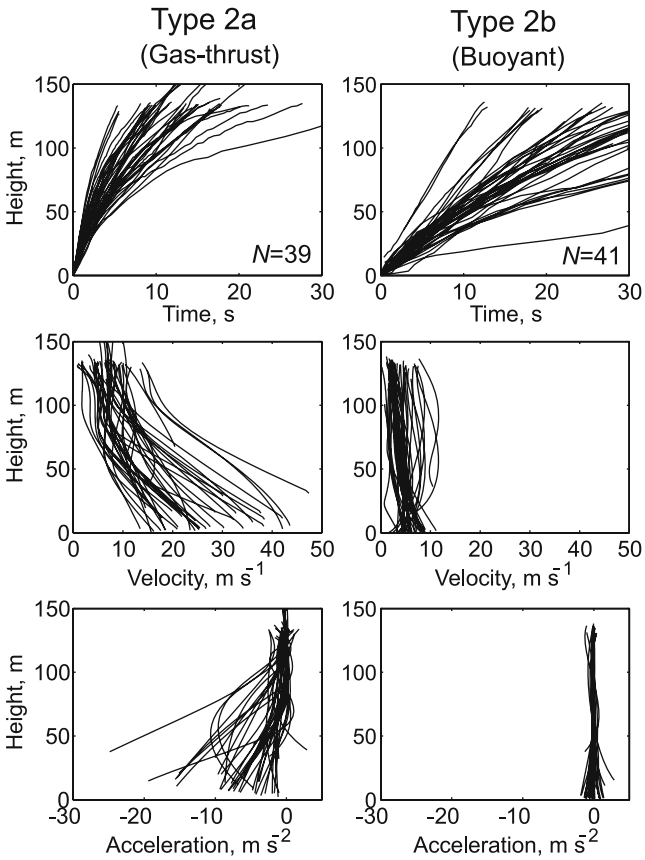

Fig. 5 Observed height, velocity and acceleration for Strombolian ash plumes. Results are from NE-1 crater in June–July 2004, and separated by eruption type. Original height values are shown, while velocity and acceleration were produced from smoothed height data (fifth-order polynomial)

any significant deceleration phase and maintained roughly constant buoyant velocities throughout their observed rise. Time-averaged velocities of the 41 Type 2b profiles indicate mean buoyant velocities between 1.4 and 10.9 m s^{-1}, with an average of 4.4 m s^{-1} (st. dev.: 2.1 m s^{-1}).

Plume velocity at crater rim

Plume velocities at the crater rim ranged from 3 to 101 m s^{-1} (Table 3, Fig. 6), agreeing well with ejecta velocities measured at Stromboli by Chouet et al. (1974), Blackburn et al. (1976), Weill et al. (1992), Ripepe et al. (1993, 2001), Ripepe (1996), Hort and Seyfried (1998), and Hort et al. (2003). The overall mean velocity was 24 m s^{-1}, while Type 1 eruptions had a mean velocity of 34 m s^{-1} (range 9–101 m s^{-1}) and Type 2 eruptions had a mean of 19 m s^{-1} (range 3–58 m s^{-1}). The Type 1 velocity distribution is unimodal (20–30 m s^{-1}) and more normal than the Type 2 distribution, which is bimodal (0–10 and 20–30 m s^{-1}) and highly skewed toward lower velocities (Fig. 6). The mean Type 2a velocity is 31 m s^{-1} (range 16–58 m s^{-1}), close to the mean Type 1 velocity, but the mean Type 2b velocity is 7 m s^{-1} (range 3–11 m s^{-1}). The two Type 2 velocity modes, therefore, reflect the distinct Type 2a and Type 2b populations (Fig. 6).

The course of plume velocities at the crater rim through time, for NE-1 crater in 2004, is shown in Fig. 7. The consistency of eruption style (Type 1 or 2) among observation days suggests persistence over a timescale of days to weeks ("Style timescales and crater behavior"). Note that there is no clear correlation between day-to-day velocity changes and shifts in Type 1 vs. 2 style. Instances

Table 3 Explosion parameters for June–July 2004, NE-1 crater

	Count	Min	Max	Mean	Stdev
Overall					
Crater rim velocity, m/s	134	3	101	24	19
Maximum ballistic height, m	138	0	115*(67)		
Eruption duration, s	135	6	41	15	6
Type 1					
Crater rim velocity, m/s	47	9	101	34	21
Maximum ballistic height, m	53	37	115*(33)		
Eruption duration, s	50	6	28	14	5
Type 2					
Crater rim velocity, m/s	87	3	58	19	15
Maximum ballistic height, m	85	0	115*(34)		
Eruption duration, s	85	6	41	15	6
Type 2a					
Crater rim velocity, m/s	44	16	58	31	11
Maximum ballistic height, m	45	42	115*(34)		
Eruption duration, s	45	6	41	15	6
Type 2b					
Crater rim velocity, m/s	43	3	11	7	2
Maximum ballistic height, m	40	0	96	16	24
Eruption duration, s	40	8	31	15	6

*Ejecta extended above the minimum field of view, 115 m, in (*X*) eruptions

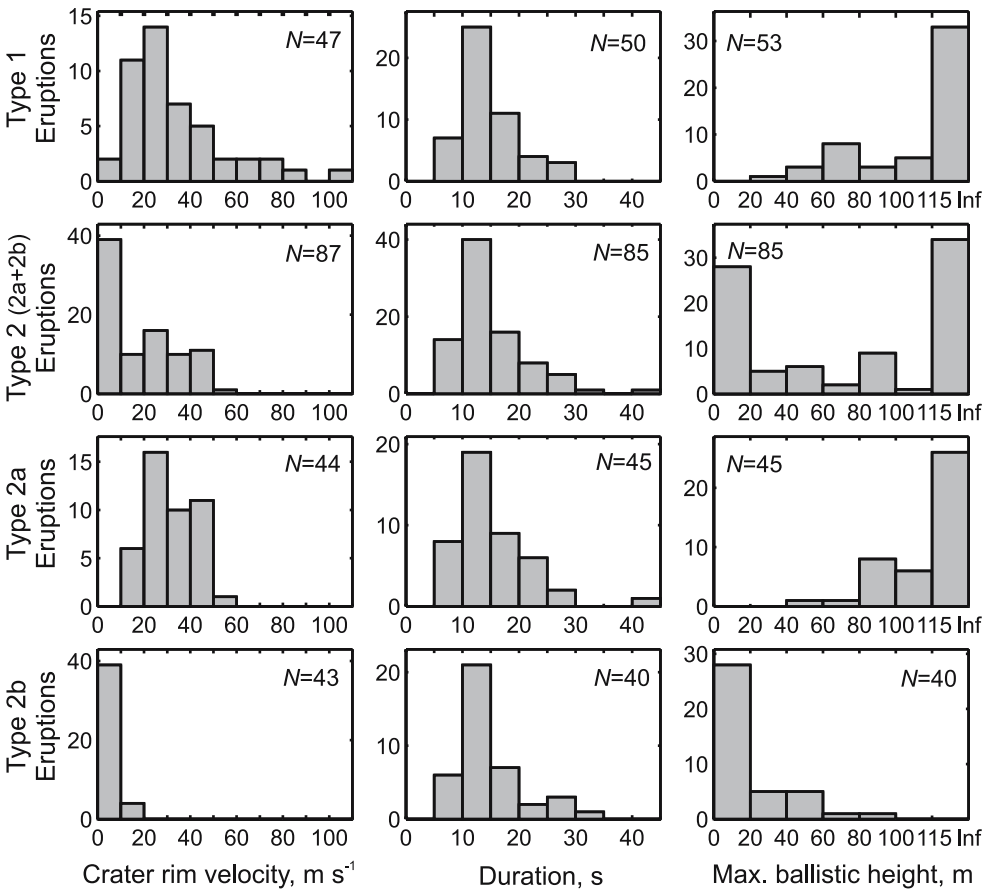

Fig. 6 Plume velocity at crater rim, eruption duration and maximum ballistic height results. Histograms show parameters for NE-1 crater eruptions captured by the FLIR during the June–July 2004 field season

in which Type 1 and 2 styles occurred on the same day (July 18 and 25) are discussed in "Style timescales and crater behavior".

Maximum ballistic height

Table 3 and Fig. 6 show that a large percentage (62%) of the Type 1 ballistics exceeded the minimum field of view (115 m height), while a smaller proportion (40%) of Type 2 ballistics did the same. Type 2a eruptions account for all of the Type 2 ballistics which exceeded 115 m (Fig. 6). As with velocity, the Type 2 height histogram is bimodal; Type 2b eruptions represent the bulk of the lowest mode (0–10 m), and high energy Type 2a eruptions form the high mode (>115 m). The daily trend of maximum ballistic height shows that ballistic height simply reflects initial velocity recast to a scale that is limited by the field of view (Fig. 7). Velocities at the crater rim greater than ~20 m s^{-1}, which account for a large portion of our eruptions, generally threw particles above 115 m.

Eruption duration

Eruptions had an overall mean duration of 15 s (range 6–41 s), and eruption duration was relatively similar among the different styles. Type 1 eruptions had a mean duration of 14 s (range 6–27 s), while Type 2 eruptions had a mean of 15 s (range 6–41 s) (Table 3; Fig. 6). Type 2a eruptions had a mean duration of 15 s (range 6–41 s), and Type 2b, 15 s (range 8–31 s) (Fig. 6). The daily trend of eruption durations for NE-1 crater in 2004 shows no significant variation in values for Type 1 or 2 eruptions (Fig. 7), or for Type 2a versus 2b eruptions. Our results agree reasonably well with those of Hort et al. (2003), who measured a mean duration between 8 and 15 s for 702 eruptions from NE crater. On a related note, the eruption frequencies during Type 1 and Type 2 phases were not significantly different. For NE-1 crater the mean Type 1 eruption frequency was 3.8 (st. dev. 0.6) eruptions $hour^{-1}$, while the mean Type 2 frequency was 4.0 (st. dev. 1.0) eruptions $hour^{-1}$.

Discussion

Origin of Type 1 and 2 styles

The Type 1 eruption style follows the common perception of strombolian eruptions: an ejection of coarse, incandescent scoria following roughly ballistic trajectories. These initially molten clots have been explained as fragments

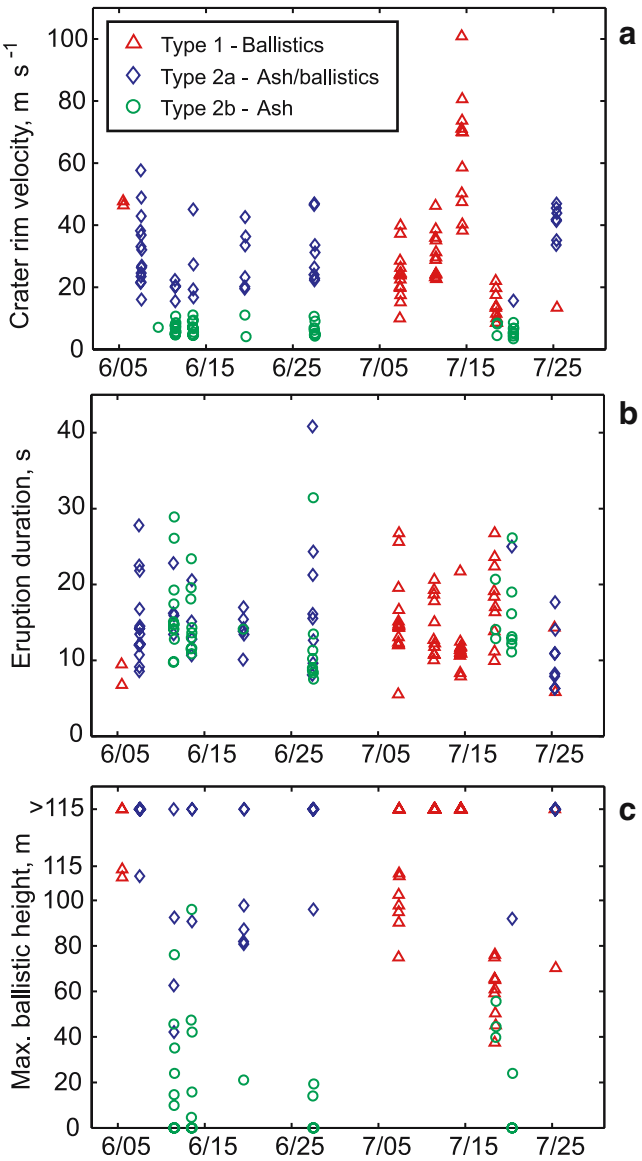

Fig. 7 Plume velocity at crater rim (**a**, 134 eruptions), eruption duration (**b**, 134 eruptions) and ballistic height through time (**c**, 138 eruptions) captured by the FLIR during the June–July 2004 field for NE-1 crater

of the fluid lava forming the slug wall (Walker 1973; Blackburn et al. 1976). Type 2 behavior, in which a fine particle plume dominates, cannot be explained in the same way. Fine fragmentation (i.e. Type 2 activity) is normally a minor component in strombolian scenarios (Self et al. 1974; Walker 1973) due to limitations in the underlying eruption mechanism. Whereas plinian eruptions produce fine particles through the disruption of many small bubbles, strombolian eruptions normally originate from the bursting of a large gas slug in a fluid magma column, where magma is torn into coarse molten particles. Fine particles, and resulting ash plumes (i.e. Type 2 activity), have thus been explained in strombolian scenarios by either (a) backfilling of loose material from above or (b) rheological changes to the magma column (references to follow).

First, backfilling of the conduit may occur through either (a) slumping of the inner crater walls or (b) rollback of explosion ejecta down the inner crater slopes toward the vent. Comminution to fine particles could be effected by subsequent explosions, ejecta impacting and rolling, or ball-milling in the conduit (Francis 1993). Backfilling has been observed directly in a few studies to create fine particle plumes (Murata et al. 1966; Booth and Walker 1973; Self et al. 1974) and inferred in several more (Heiken 1978; Guest 1982; Houghton and Schmincke 1989; Calvari and Pinkerton 2004). Calvari and Pinkerton (2004) further noted how slumping can be encouraged by a drop in magma level. The backfill mechanism is depicted in Fig. 8.

Second, increasing the viscosity of the magma may lead to fragmentation at a finer scale, and this theory has been supported recently through physical studies of ejecta. Taddeucci et al. (2002, 2004) linked a transition at Etna in 2001 from strombolian activity to quasi-vulcanian explosions with increasing crystallinity of the magma and inferred increases in magma viscosity, resulting in brittle

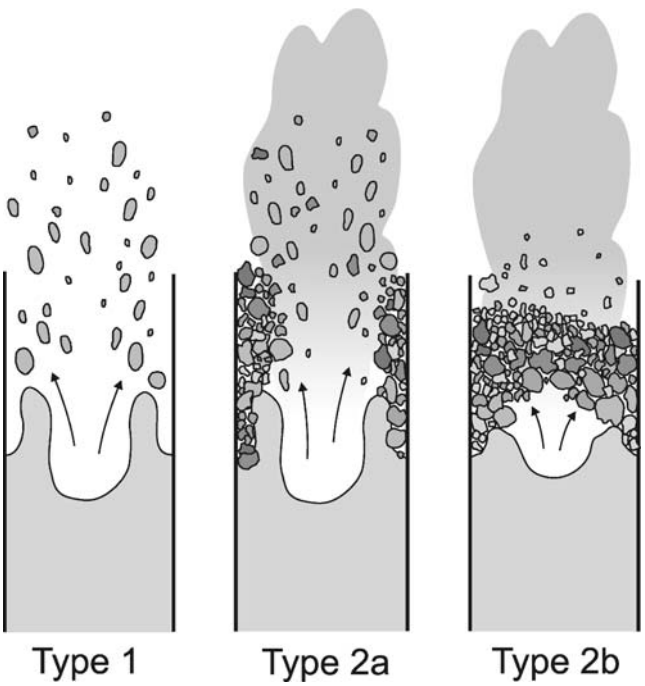

Fig. 8 Loose, brittle backfill sitting atop the magma column is one of two scenarios that can lead to ash-rich strombolian eruptions (the other scenario, rheological changes due to degassing, is not depicted in this figure). Type 1: gas slug bursts at unobstructed free surface, ejecting coarse ballistics. Type 2a: high overpressure slug burst produces large scale disruption of backfill, producing ash and ballistics. Type 2b: low overpressure slug burst results in minor disruption of loose backfill, creating ash but few ballistics

fracturing of the uppermost magma column. Valentine et al. (2005) recorded increases in crystallinity and inferred viscosity in ash-rich strombolian deposits, and speculated how higher viscosity melt may inhibit decoupled gas rise (i.e. hinder slug formation), producing small bubbles and fine fragmentation. One component of their model, a sustained eruption column, clearly does not apply to our Type 2 eruptions. Lautze and Houghton (2005) showed how shallow melt at Stromboli can exhibit different degrees of degassing, and discuss how variations in rheology may be linked to changes in eruption style.

With imaging alone it is difficult to discriminate which of these mechanisms is the main cause of fine-scale fragmentation, and our study cannot favor one general mechanism (backfilling vs. rheology) over another. Even if rigorous physical sampling were to be coupled with imaging, however, several complications exist in separating the mechanisms. First, particles created from both mechanisms may be ejected together, because the two mechanisms can easily be coupled. One can imagine that during any phases of weak strombolian activity the magma flux to the surface will decrease, favoring higher viscosities in the shallow melt due either to greater cooling or increased degassing. At the same time, the weak explosive energy will reduce ejecta dispersal (more particles falling within the crater rim, encouraging rollback), and the ability for vent-clearing, leading to backfill accumulation as well. The second complication is one that may exist in identifying the backfill mechanism. Recognizing fine particles produced by the backfill mechanism would likely rely on the chemical or physical degradation that results from a significant residence in the conduit. This requires that the turnover timescale be significant as well, which may not always be the case. In other words, particles which are recycled from an eruption 10 min earlier may not bear any imprint of the recycling beyond secondary fragmentation, and thus may be interpreted incorrectly as derived directly from the magma column.

Observed transition timescales, however, can sometimes play a valuable part in the interpretation. For instance, a sustained Type 1 phase which is briefly interrupted by a Type 2 phase would be strong evidence of a discrete slump of material into the conduit. This occurred on 18 July 2004, and is discussed in "Style timescales and crater behavior." This 1 h Type 2 phase argues against a rheological mechanism—at least in this rare instance—and it likely reflects a small-scale collapse of material onto the vent that was rapidly cleared.

The height of the magma column may control Type 1 and 2 behavior in encouraging the backfilling scenario; a drop in magma level would allow slumping of unsupported loose material into the vent (Calvari and Pinkerton 2004). If we use particle collimation as an indicator of magma depth, the data in our study are ambiguous in this regard. The best (Fig. 4e) and most poorly (Fig. 4a) collimated explosions were Type 1 eruptions. The best collimated explosions comprised the highest velocities we recorded, suggesting that velocity may also play a role in collimation.

Weather (temperature, humidity, rain recorded at the summit weather station every 30 min) did not have any obvious relation with the transitions observed during this period; the weather was generally stable during the two-month observation period. Rain was recorded only on June 17, and did not occur with any obvious changes in activity, although there was a large gap in weather data during 01–16 July. The fact that significant changes in eruptive styles were observed in our dataset in the absence of notable weather fluctuations may argue against theories in which weather is a primary control on eruption style (Urbanski et al. 2002; Hort et al. 2003). On the other hand, heavy rains could encourage backfill accumulation by washing loose material onto the vent, as Urbanski et al. (2002) noted.

Origin of Type 2a and 2b styles

Type 2a eruptions involve a visible gas thrust phase as well as many ballistic particles, whereas Type 2b eruptions involve only buoyant velocities visible above the crater rim and a minor amount of ballistics. Given only the height vs. time profiles in Fig. 5, it is tempting to think that Type 2b plumes reflect a drop in magma-level, so that the gas thrust phase was hidden below the crater rim. This is clearly not the case, however, as Type 2a and 2b eruptions were interlaced in time on a scale of seconds to minutes, which is much shorter than reasonable timescales for magma level changes of ~75–100 m (gas thrust heights in Type 2a plumes).

In addition, infrasonic pressure was recorded for 74 of the 93 Type 2 NE-1 eruptions by University of Firenze microphones (Ripepe et al. 2004, 2005), with results shown in Fig. 9. Eruptions in which the infrasonic amplitude did not noticeably exceed the background (~1 Pa) were assigned a value of 0, and this was more common with Type 2b eruptions (73%) than with Type 2a eruptions (15%). Figure 9 indicates that Type 2a eruptions were prone to higher infrasonic amplitudes than Type 2b eruptions, indicating that Type 2a eruptions generally involve greater bubble overpressures. The higher abundance of ballistic particles and the higher velocities in Type 2a vs. Type 2b eruptions is, therefore, consistent, as both ballistic particles and the ash plume rely on the bubble overpressure for their initial velocities. In other words, higher energy explosions (Type 2a) will have the ability to cast coarse particles to greater heights (see ballistic heights in Fig. 6).

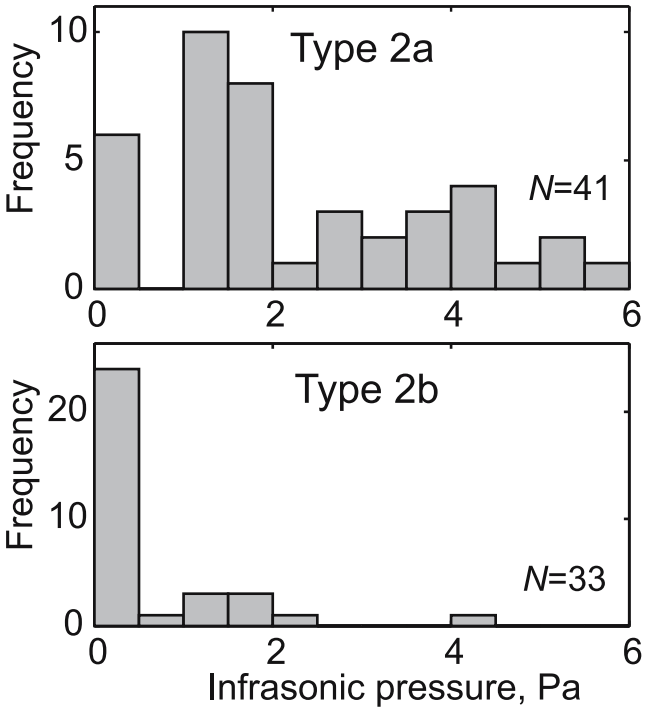

Fig. 9 Infrasonic amplitudes at ROC (450 m distance) for 74 eruptions from NE-1 crater. Type 2a eruptions are prone to higher amplitudes, suggesting greater bubble overpressures

NE and SW craters

Anecdotal evidence, gathered from those who have worked on the volcano for years to decades (authors M.R. & A.J.L. H), indicates that Type 1 and Type 2 activity are both quite common at Stromboli. Type 2 activity is not as prevalent as Type 1 activity, and it is typically associated with SW crater. These observations are in contrast to our dataset of 344 eruptions, in which 64% of the total number were Type 2 style, of which slightly more than half (122) originated from NE crater. We speculate that this disproportionate number of Type 2 eruptions may be due to atypical circumstances during the time of our two main datasets, May 2002 and June–July 2004. In May 2002, activity was at a low intensity (Smithsonian Institution 2002), and 61% of the 64 eruptions were Type 2. Reduced explosivity would limit the dispersal of ballistic clasts and result in more material falling within the crater walls and accumulating on top of the vent. Low explosive energy would also hamper the ability to clear any buildup. These conditions would encourage backfill buildup and Type 2 behavior.

The June–July 2004 activity was generally moderate in intensity, with 71% of the 240 eruptions being Type 2. Following the December 2002 crater terrace collapse, the craters were in a prolonged constructional phase since strombolian activity resumed toward the end of the effusive phase in July 2003 (Calvari et al. 2005; Ripepe et al. 2005). NE-1 crater developed a nascent cinder cone between June 2003 and June 2004 within the collapsed walls of the crater terrace (Fig. 10), and the remaining obscured vents likely featured similar constructs. The growing craters were probably less stable than they would be in an established steady state, potentially leading to increased slumping and backfill accumulation. In addition, each crater is nested tightly within the indurated outer structure of the crater terrace. A typical cinder cone on a nominally flat surface contains most of its material in the outer walls (McGetchin et al. 1974). At Stromboli, and clearly visible at NE-1 crater, the outer walls of the cones would be truncated by the outer structure. This would lead to accelerated upward growth and, therefore, increased collapse frequency and resultant Type 2 behavior.

Anecdotal information and several studies (Chouet et al. 1999, 2003; Ripepe and Marchetti 2002; Marchetti and Ripepe 2005) covering more typical phases of activity at Stromboli points to Type 2 behavior being more common

Fig. 10 Cone construction in NE crater. Following the end of the 2002–2003 effusive phase (July 2003), the collapsed crater terrace (*top*) began rebuilding itself. By June 2004, a nascent cinder cone had developed in NE-1 crater. Top photo courtesy of Elske de Zeeuw-van Dalfsen

at SW crater than NE crater, in general. Considering the effects that backfill can have on eruption style, this distinction is consistent with the gas overpressure differences measured for the two craters. Ripepe and Marchetti (2002) indicated that the average bubble overpressure is ~0.5 b for SW crater and ~4 b for NE crater. The lower overpressures of SW crater would limit ejecta dispersal and thus increase rollback, while reducing vent-clearing, favoring backfill accumulation. Anecdotal information also mentions SW crater's occasional red ash plumes, presumably oxidized material that further supports a backfill origin for the ash-charged activity at this vent.

Strombolian classification

This work explores the variability in eruption styles at Stromboli, aided by the ability of longwave infrared imagery to record a wide range of ejecta components. Nevertheless, many other studies have noted variations in eruption styles at Stromboli. Ripepe et al. (1993, 2001) and Ripepe (1996) showed how eruptions could be divided into two types, in which one was short and impulsive and the other longer and less impulsive. Impulsive ballistic-rich eruptions are commonly attributed to NE crater and emergent ash-rich eruptions to SW crater (Chouet et al. 1999, 2003; Ripepe and Marchetti 2002; Marchetti and Ripepe 2005). Our data show that both ballistic-rich and ash-rich eruptions can occur at both craters, though anecdotal evidence and these previous studies point to Type 2 activity being more common at SW crater.

Our collection of imagery reinforces the view that strombolian eruption styles can vary widely in appearance. Due to aforementioned limitations in imaging technology and dataset size, previous studies may not have sufficiently illustrated or explored this range of behavior. This has made it difficult to appreciate that two seminal works on strombolian activity, Chouet et al. (1974) and Blackburn et al. (1976), were analyzing two very different eruption styles. Chouet et al. (1974) described 'molten lava fragments' and 'small quantities of ash,' suggestive of Type 1 activity, while Blackburn et al. (1976) mentioned the 'convective cloud of gas and small pyroclasts' consistent with Type 2 style. These are often cited interchangeably in the literature, when it should be clear that each was studying a distinct aspect of strombolian eruptive behavior.

Our results also illustrate an exception to the common maxim that finer fragmentation necessarily results from more violent explosive activity. For example, the rigorous analysis of cone-building strombolian deposits at numerous volcanoes by Walker (1973) identified minor components of fine fragmentation which were assumed to be related to 'violent' strombolian behavior. The average buoyant plume velocities we observed (1.4–10.9 m s^{-1}) in our dataset equate to terminal velocities for particle sizes of ~0.1–8.8 mm (using a drag coefficient of 1 and density of 1,100 kg m^{-3}), suggesting there is a significant amount of material fragmented to less than 1 mm in many of these plumes. As we have shown, this fine fragmentation is present during periods of normal strombolian explosive intensity (Figs. 6 and 7). Agreeing with Self et al. (1974), our results suggest that, in general, some fine proximal strombolian deposits could be related to Type 2 phases of normal intensity strombolian activity. Type 2 eruptions may also provide a mechanism consistent with the fine-grained cone construction modeled by Riedel et al. (2003).

Conclusions

We imaged 344 eruptions at Stromboli volcano, Italy, with a FLIR thermal video camera. These data provide a new and powerful means to unravel the dynamics of explosive events. The specific insights provided by this work are summarized as follows:

(1) Eruptions at Stromboli exhibit a wide range of styles, and explosions can be dominated by ballistic particles (Type 1) or ash (Type 2). Type 2 eruptions can be subdivided into Type 2a style, which exhibits a visible gas thrust phase (>15 m s^{-1}) and significant ballistic particles, and Type 2b style which shows only convective velocities (<15 m s^{-1}) above the crater rim and a minor amount of ballistics.

(2) Type 1 eruptions imply a normal strombolian magma column, while Type 2 eruptions indicate either (a) backfilled material in the conduit or (b) rheological changes to the magma. Infrasonic pressures indicate that Type 2a and 2b eruptions are caused by varying levels of bubble overpressure. Changes in eruption style did not seem to be caused by weather fluctuations during our observation period.

(3) Overall, these imaging data cannot favor one mechanism over another (backfilling vs. rheological changes), though backfilling was inferred in at least one instance.

(4) Individual vents at Stromboli maintain Type 1 and Type 2 phases on a timescale of days to weeks, indicating that backfilling or rheological changes exhibit cycles on that timescale. Type 2a and 2b eruptions could appear within minutes of each other, because bubble overpressure can vary significantly on that timescale.

(5) SW crater may be prone to Type 2 behavior due to its typically lower gas overpressures (allowing backfill

accumulation), while NE crater may be prone to Type 1 behavior due to its higher gas overpressures (enabling vent clearing).

(6) Type 2 behavior suggests that some fine-grained proximal strombolian deposits may result from normal intensity strombolian activity, not necessarily more explosive, or 'violent,' strombolian activity.

Our quantitative results were limited in two ways. First, our inability to extract quantitative information from SW crater eruptions limited our quantitative results to NE crater. Second, our results were limited by the short acquisition periods (~4 h); continuous acquisition by a remotely operated camera, over weeks to months, could provide a complete picture of eruption style transitions.

Our insights on the causes of eruption style transitions could also be improved. First, systematic collection of ejecta (Lautze and Houghton 2005; Taddeucci et al. 2004) coupled directly with FLIR imaging could help determine the role of rheology in eruption style changes, even considering the challenges discussed in "Origin of Type 1 and 2 styles." Second, direct imaging of the vent region—though hazardous—could unravel the ambiguity surrounding the role of magma level fluctuations, clast avalanching, and ejecta accumulation on eruption style.

Previous FLIR studies have largely focused on effusive volcanic activity (e.g. Wright and Flynn 2003; Calvari et al. 2005), and this paper marks one of the first rigorous studies of explosive activity with the FLIR camera. We have shown how the FLIR can provide an improved view of different ejecta components compared to visible or near-infrared imagery. The coarse pixel size, however, is a primary shortcoming of the FLIR.

Finally, this study focused on eruption styles and dynamics using the spatio-textural information in the image. We did not explicitly examine the temperature information available in the FLIR data, and future work will exploit this aspect to investigate eruption thermodynamics in detail.

Acknowledgements This paper benefited greatly from discussions with N. Lautze, B. Houghton, L. Wilson, J. Hammer, L. Flynn, R. Wright, S. Fagents, S. Baloga, S. Self and J. Sumner. We thank J. Gagnon and B. Risser of FLIR Systems, Inc. for technical information regarding the cameras and G. Salerno (INGV) for weather data. J.L. Palma shared insights from his participation in the 2004 field campaign. We thank the Italian Department of Civil Protection for logistical support at Stromboli. Reviews by D. Swanson, R. Scandone, and an anonymous reviewer are greatly appreciated. This work was supported by NSF grant no. EAR-0207734, NERC grant no. NER/B/S/2001/00707, the USGS Volcano Hazards Program and the Geophysical Institute at the University of Alaska Fairbanks.

References

Allard P, Carbonnelle J, Metrich N, Loyer H, Zettwoog P (1994) Sulphur output and magma degassing budget of Stromboli volcano. Nature 368:326–330

Blackburn EA, Wilson L, Sparks RSJ (1976) Mechanisms and dynamics of strombolian activity. J Geol Soc London 132:429–440

Booth B, Walker GPL (1973) Ash deposits from the new explosion crater, Etna 1971. Phil Trans R Soc London A274:147–161

Calvari S, Pinkerton H (2004) Birth, growth and morphologic evolution of the "Laghetto" cinder cone during the 2001 Etna eruption. J Volcanol Geotherm Res 132:225–239, DOI 10.1016/S0377-0273(03)00347-0

Calvari S, Spampinato L, Lodato L, Harris AJL, Patrick MR, Dehn J, Burton MR, Andronico D (2005) Chronology and complex volcanic processes during the 2002–2003 flank eruption at Stromboli volcano (Italy) reconstructed from direct observations and surveys with a handheld thermal camera. J Geophys Res 110: B02201, DOI 10.1029/2004JB003129

Chouet B, Hamisevicz N, McGetchin TR (1974) Photoballistics of volcanic jet activity at Stromboli, Italy. J Geophys Res 79:4961–4976

Chouet B, Saccorotti G, Dawson P, Martini M, Scarpa R, De Luca G, Milana G, Cattaneo M (1999) Broadband measurements of the sources of explosions at Stromboli volcano. Geophys Res Lett 26:1937–1940

Chouet B, Dawson P, Ohminato T, Martini M, Saccorotti G, Giudicepietro F, De Luca G, Milana G, Scarpa R (2003) Source mechanisms of explosions at Stromboli Volcano, Italy, determined from moment-tensor inversions of very-long-period data. J Geophys Res 108:2019, DOI 10.1029/2002JB001919

Dehn J, Harris AJL, Ripepe M (2001) Infrared imaging of Strombolian eruptions. Eos Trans AGU 82(47) (Fall Meet Suppl, V52C-01)

Foshag WF, Gonzalez-Reyna J (1956) Birth and development of Paricutin volcano. US Geol Surv Bull 965-D:355–489

Francalanci L, Tommasini S, Conticelli S (2004) The volcanic activity of Stromboli in the 1906–1998 AD period: mineralogical, geochemical and isotope data relevant to the understanding of the plumbing system. J Volcanol Geotherm Res 131:179–211, DOI 10.1016/S0377-0273(03)00362-7

Francis P (1993) Volcanoes—a planetary perspective. Oxford University Press, Oxford

Giberti G, Jaupart C, Sartoris G (1992) Steady-state operation of Stromboli volcano, Italy: constraints on the feeding system. Bull Volcanol 54:535–541

Guest JE (1982) Styles of eruption and flow morphology on Mt Etna. Mem Soc Geol Ital 23:49–73

Harris AJL, Stevenson DS (1997) Magma budgets and steady-state activity of Vulcano and Stromboli. Geophys Res Lett 24:1043–1046

Heiken G (1978) Characteristics of tephra from Cinder Cone, Lassen Volcanic National Park, California. Bull Volcanol 41:119–130

Hort M, Seyfried R (1998) Volcanic eruption velocities measured with a micro radar. Geophys Res Lett 25:113–116

Hort M, Seyfried R, Voge M (2003) Radar Doppler velocimetry of volcanic eruptions: theoretical considerations and quantitative documentation of changes in eruptive behavior at Stromboli volcano, Italy. Geophys J Int 154:515–532, DOI 10.1046/j.1365-246X.2003.01982.x

Houghton BF, Schmincke H-U (1989) Rothenberg scoria cone, East Eifel: a complex Strombolian and phreatomagmatic volcano. Bull Volcanol 52:28–48

Jaupart C, Vergniolle S (1988) Laboratory models of Hawaiian and Strombolian eruptions. Nature 331:58–60

Kirchdorfen M (1999) Analysis and quasistatic FE modeling of long period impulsive events associated with explosions at Stromboli volcano (Italy). Ann Geophys 42:379–391

Lautze N, Houghton BF (2005) Physical mingling of magma and complex eruption dynamics in the shallow conduit at Stromboli volcano, Italy. Geology 33:425–428, DOI 10.1130/G21325.1

Macdonald GA (1972) Volcanoes. Prentice-Hall, Englewood Cliffs, NJ

Marchetti E, Ripepe M (2005) Stability of the seismic source during effusive and explosive activity at Stromboli Volcano. Geophys Res Lett 32:L03307, DOI 10.1029/2004GL021406

McGetchin TR, Chouet BA (1979) Energy budget of the volcano Stromboli, Italy. Geophys Res Lett 6:317–320

McGetchin TR, Settle M, Chouet BA (1974) Cinder cone growth modeled after Northeast Crater, Mount Etna, Sicily. J Geophys Res 79:3257–3272

Murata KJ, Dondoli C, Saenz R (1966) The 1963–65 eruption of Irazú Volcano, Costa Rica (The period of March 1963 to October 1964). Bull Volcanol 29:765–796

Ntepe N, Dorel J (1990) Observations of seismic volcanic signals at Stromboli volcano (Italy). J Volcanol Geotherm Res 43:235–251

Parfitt EA (2004) A discussion of the mechanisms of explosive basaltic eruptions. J Volcanol Geotherm Res 134:77–107, DOI 10.1016/j.jvolgeores.2004.01.002

Parfitt EA, Wilson L (1995) Explosive volcanic eruptions—IX. The transition between Hawaiian-style lava fountaining and Strombolian explosive activity. Geophys J Int 121:226–232

Patrick M (2007) Dynamics of strombolian ash plumes from thermal (FLIR) video: motion, morphology and air entrainment. J Geophys Res (in press)

Riedel C, Ernst GGJ, Riley M (2003) Controls on the growth and geometry of pyroclastic constructs. J Volcanol Geotherm Res 127:121–152, DOI 10.1016/S0377-0273(03)00196-3

Ripepe M (1996) Evidence for gas influence on volcanic seismic signals recorded at Stromboli. J Volcanol Geotherm Res 70:221–233

Ripepe M, Marchetti E (2002) Array tracking of infrasonic sources at Stromboli volcano. Geophys Res Lett 29:2076, DOI 10.1029/2002GL015452

Ripepe M, Rossi M, Saccorotti G (1993) Image processing of explosive activity at Stromboli. J Volcanol Geotherm Res 54:335–351

Ripepe M, Ciliberto S, Della Schiava M (2001) Time constraints for modeling source dynamics of volcanic explosions at Stromboli. J Geophys Res 106:8713–8727, DOI 10.1029/2000JB900374

Ripepe M, Marchetti E, Poggi P, Harris AJL, Fiaschi A, Ulivieri G (2004) Seismic, acoustic, and thermal network monitors the 2003 eruption of Stromboli volcano. Eos Trans AGU 85:329–336, DOI 10.1029/2004EO350001

Ripepe M, Marchetti E, Ulivieri G, Harris AJL, Dehn J, Burton M, Caltabiano T, Salerno G (2005) Effusive to explosive transition during the 2003 eruption of Stromboli volcano. Geology 33:341–344, DOI 10.1130/G21173.1

Self S, Sparks RSJ, Walker GPL, Booth B (1974) The 1973 Heimay strombolian scoria deposit, Iceland. Geol Mag 111:539–548

Self S, Kienle J, Huot J-P (1980) Ukinrek Maars, Alaska, II. Deposits and formation of the 1977 craters. J Volcanol Geotherm Res 7:39–65

Smithsonian Institution (2002) Stromboli volcano. Bull Glob Volcanism Netw 27:07

Sparks RSJ, Wilson L (1976) A model for the formation of ignimbrite by gravitational column collapse. J Royal Soc London 132:441–451

Sparks RSJ, Bursik MI, Carey SN, Gilbert JS, Glaze LS, Sigurdsson H, Woods AW (1997) Volcanic plumes. Wiley, Chichester

Steinberg GS, Babenko JI (1978) Experimental velocity and density determination of volcanic gases during eruption. J Volcanol Geotherm Res 3:89–98

Taddeucci J, Pompilio M, Scarlato P (2002) Monitoring the explosive activity of the July–August 2001 eruption of Mt Etna (Italy) by ash characterization. Geophys Res Lett 29:1029–1032, DOI 10.1029/2001GL014372

Taddeucci J, Pompilio M, Scarlato P (2004) Conduit processes during the July–August 2001 explosive activity of Mt Etna (Italy): inferences from glass chemistry and crystal size distribution of ash particles. J Volcanol Geotherm Res 137:33–54, DOI 10.1016/j.jvolgeores.2004.05.011

Urbanski N-A, Vöge M, Seyfried R, Rüpke L, Petersen T, Hanebuth T, Hort M (2002) Fifteen days of continuous activity survey at Stromboli volcano, Italy, in late September 2000: Doppler radar, seismicity, infrared, soil humidity and mapping of the crater region. Intl J Earth Sci 91:712–721, DOI 10.1007/s00531-001-0242-y

Valentine GA, Krier D, Perry FV, Heiken G (2005) Scoria cone construction mechanisms, Lathrop Wells volcano, southern Nevada, USA. Geology 33:629–632, DOI 10.1130/G21459.1

Vergniolle S, Brandeis G (1994) Origin of the sound generated by Strombolian explosions. Geophys Res Lett 21:1959–1962

Vergniolle S, Brandeis G (1996) Strombolian explosions. 1. A large bubble breaking at the surface of a lava column as a source of sound. J Geophys Res 101:20433–20447

Walker GPL (1973) Explosive volcanic eruptions—a new classification scheme. Geol Rundsch 62:431–446

Weill A, Brandeis G, Vergniolle S, Baudin F, Bilbille J, Fevre J-F, Piron B, Hill X (1992) Acoustic sounder measurements of the vertical velocity of volcanic jets at Stromboli volcano. Geophys Res Lett 19:2357–2360

Wilson L (1980) Relationships between pressure, volatile content, and ejecta velocity in three types of volcanic explosions. J Volcanol Geotherm Res 8:297–313

Wright R, Flynn LP (2003) On the retrieval of lava-flow surface temperatures from infrared satellite data. Geology 31:893–896, DOI 10.1130/G19645.1